

Variation of stress intensity factor along a small interface crack front in singular stress fields



Hideo Koguchi^{a,*}, Koki Yokoyama^b, Chonlada Luangarpa^a

^a Nagaoka University of Technology, 1603-1 Kamitomioka, Nagaoka, Niigata 940-2188, Japan

^b Graduate School of Nagaoka University of Technology, 1603-1 Kamitomioka, Nagaoka, Niigata 940-2188, Japan

ARTICLE INFO

Article history:

Received 5 February 2015

Received in revised form 9 May 2015

Available online 6 July 2015

Keywords:

Three-dimensional joints

Interface crack

Singular stress

Stress intensity factor

Eigenanalysis

Boundary element analysis

ABSTRACT

Stress singularities usually occur at vertexes in three-dimensional joints. Cracks frequently initiate at the vertex, and the joint fails under an external force or a thermal load. In the present study, the stress distribution near a small crack occurring at a vertex in a three-dimensional joint under a tensile load is examined, and the stress intensity factors at the crack tip are investigated along the crack tip front. The joint is made of Si and resin. In the analysis, three kinds of crack shapes (triangular, quarter circular, and concave) are supposed as the initial crack shape. The stress distribution around the crack is normalized using the singular stress near the vertex since the crack exists in the singular stress field. The stress intensity factor varies along the crack tip from the inner point to the free surface. The value of the stress intensity factor varies following the order of the stress singularity at the point of the free surface. In this analysis, the stress intensity factor is expressed as a function of the distance from the cross point of the free surface and the crack tip. Specifically, the function is composed of an exponential function of the difference between the order of the stress singularity at the cross point and the crack tip.

© 2015 Elsevier Ltd. All rights reserved.

1. Introduction

It is well known that singular stress fields occur at the corners of joint interfaces between dissimilar materials due to the mismatch of their material properties. When an external force or a temperature change is applied to such a joint, a crack occurs at or near the interface due to the singular stress field; this frequently results in the failure of the joint. On the stress singularity, Williams (1959) derived an exact solution for elastic solids with an interface crack and reported rapid oscillations in the stress and displacement fields.

$$\begin{aligned} [\sigma_{yy} + i\tau_{xy}]_{\theta=0} &= \frac{K_1^* + iK_2^*}{\sqrt{2\pi r}} \left\{ \cos\left(\varepsilon \ln \frac{r}{\ell}\right) + i \sin\left(\varepsilon \ln \frac{r}{\ell}\right) \right\} \\ \delta_y + i\delta_x &= \frac{K_1^* + iK_2^*}{2(1+2i\varepsilon) \cosh(\varepsilon\pi)} \left\{ \frac{\kappa_1 + 1}{\mu_1} + \frac{\kappa_2 + 1}{\mu_2} \right\} \left(\frac{r}{2\pi} \right)^{\frac{1}{2}} \left(\frac{r}{\ell} \right)^{i\varepsilon} \\ \varepsilon &= \frac{1}{2\pi} \ln \left(\frac{1-\beta}{1+\beta} \right) \end{aligned} \quad (1)$$

where β is a dimensionless composite parameter depending on the material properties introduced by Dundurs (1969).

Here, K_1^* and K_2^* are the parameters for characterizing the near tip field of the interface crack, r is the distance from the crack tip, and ℓ represents a reference length. When the two materials are identical $\varepsilon = 0$, the factors K_1^* and K_2^* becomes identical to K_I for the mode I (tensile opening) and K_{II} for the mode II (plane shear), respectively.

Subsequently, Sih et al. (1962) conducted an analysis of stress singularity at crack tips in plane problems and bending problems using a complex variable method. Rice and Sih (1965) proposed the stress intensity factors k_1 and k_2 for an interface crack of length $2a$ under a uniform tensile load P . For the same problem, Erdogan (1965) proposed a complex stress intensity factor. Rice (1988) reexamined elastic fracture mechanics for a crack on the interface between dissimilar solids. Hutchinson and Suo (1991) indicated that the real and imaginary parts of the complex stress intensity factor correspond to modes I & II for an ordinary crack, respectively. Miyazaki et al. (1993) analyzed the stress intensity factors of interface crack using a boundary element method. Qu and Bassani (1993) developed the fracture mechanics of interface cracks in anisotropic bimetals and derived explicit expressions for the crack-tip fields and the associated stress intensity factors. It is very important to evaluate the stress intensity factor for a small crack at the vertex in the singular stress field for estimating the real strength of joints. Akisanya and Fleck (1997) performed

* Corresponding author.

E-mail addresses: koguchi@mech.nagaokaut.ac.jp (H. Koguchi), s113105@stn.nagaokaut.ac.jp (K. Yokoyama), chonlada@mech.nagaokaut.ac.jp (C. Luangarpa).

stress analysis for a crack at the interface edge in a two-dimensional joint and demonstrated that the stress intensity factor became large for a short crack due to the effect of singular stress fields and reduced for a long crack. Bjerken and Persson (2001) presented a method for obtaining the complex stress intensity factor for an interface crack in a bimaterial using a minimum number of computations. Ioka et al. (2002) conducted stress analysis in a two-dimensional joint with a small crack at the edge of the interface and investigated the effect of the singular stress field on the stress at the crack tip. Sukumar et al. (2004) presented a method for determining the complex stress intensity factor for an interface crack in two-dimensional joints using an enriched finite element. Leguillon et al. (2003) an Irwin-like criterion was used to examine the failure of two steel plates bonded together by an epoxy joint. They discussed several criteria for crack initiation at sharp notches and tried to propose a simple and robust criterion to predict brittle crack initiation at bond ends. Johnson and Qu (2007) proposed a method for calculating the stress intensity factor of an interface crack under a temperature gradient by evaluating the path-independent integral around the crack tip region using the finite element method. Recently, Hirai et al. (2012) presented an extension of the Stroh formalism and the H -integral derived from Betti's reciprocal principle for piezoelectric problems. They proposed a new definition of the SIFs of an interfacial corner for piezoelectric materials. Hwu and Huang (2012) presented a definition of the stress intensity factors for interface corners including interface cracks. On three-dimensional singularities and cracks, Lee et al. (1987) calculated the stress intensity factors for a crack of arbitrary planar shape near a bimaterial interface using the body-force method. Ghahremani and Shih (1992) investigated singular stress fields near the intersection of a planar interfacial crack with the free surface in joined materials. Nakamura and Kamath (1992) conducted a three-dimensional finite element analysis of the mechanics of crack growth and decohesion in a highly compliant thin film bonded to a rigid substrate. Gosz et al. (1998) developed new domain integrals for extracting mixed-mode stress intensity factors along curved three-dimensional bimaterial interface cracks. In the derivation, the asymptotic auxiliary fields for the plane problem of a bimaterial interface crack were imposed along a curved crack front. Begley and Ambrico (2001) presented the mechanics governing delamination of thin films driven by thermal expansion mismatch from two-dimensional interface flaws. Results were presented for energy release rates and mode-mixity along two-dimensional crack fronts. Song and Wolf (2002) developed a scaled boundary finite-element method, a semi-analytical boundary-element method based on finite elements, for analyzing fracture mechanics problems. Zhou et al. (2005) proposed a new three-dimensional variable-order singular boundary element for stress analysis of three-dimensional interface cracks and internal material junctions. Ortiz and Cisilino (2005) presented a general numerical tool for the analysis of three-dimensional bimaterial interface cracks. Ayhan et al. (2006) developed an efficient computational technique that utilizes enriched crack tip elements containing the correct interface crack tip asymptotic behavior. In the enriched element formulation, the stress intensity factors K_I , K_{II} , and K_{III} were treated as additional degrees of freedom and were obtained directly during the finite element solution phase. Tvergaard and Hutchinson (2008) investigated the effect of modes I, II, and III on interface crack growth. Chiu and Lin (2009) investigated the variation in the stress intensity factor, energy release rate, and phase angle along the front of a crack using a virtual growth method for a three-dimensional interface crack in electronic devices. Nagai et al. (2007) calculated the stress intensity factor for a three-dimensional interface crack in dissimilar anisotropic materials. Recently, Veluri and Jensen (2013) presented a

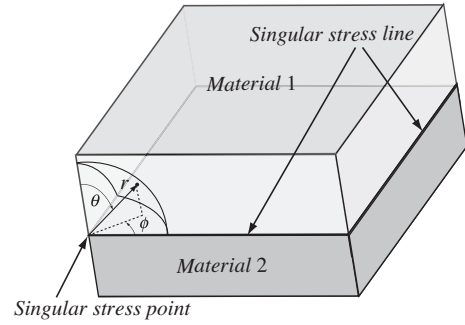


Fig. 1. Singular stress point and singular line in a three-dimensional joint.

method for determining the shape of a growing interface crack between a thin film and a substrate by means of a commercial finite element program.

There are few papers on three-dimensional interface cracks under a complicated stress state such as the singular stress field. The authors investigated the characteristics of singular stress fields at the vertex of the interface in three-dimensional joints (Koguchi et al., 2012) and in particular, the relationship between singular stress lines and a three-dimensional singular stress field (Koguchi and da Costa, 2010). In the three-dimensional stress singularity field, the stress fields can be expressed as

$$\sigma_{ij}(r, \theta, \phi) = \sum_{l=1}^m K_l f_{ijl}(\theta, \phi) r^{-\lambda_l} + K_{m+1} f_{(m+1)ij}(\theta, \phi) + K_{m+2} f_{(m+2)ij}(\theta, \phi) \ln r \quad (2)$$

where K_l represents the l th intensity of the singularity, $f_{ijl}(\theta, \phi)$ is the angular function of the l th value of the stress singularity, and r is the distance from the singular stress point (see Fig. 1).

Cracks frequently initiate at the singular stress point of the vertex in three-dimensional joints. Koguchi and Kimura (2014) calculated the energy release of a small crack at an initial stage of crack occurrence in a singular stress field. In several papers (Nagai et al., 2007; Kuo and Hwu, 2010) on three-dimensional interface cracks, the definition of the stress intensity factor for the generalized plane strain condition on the basis of the two-dimensional anisotropic elasticity was employed. In the present paper, a stress intensity factor corresponding to a complex angular function for a complex singularity is defined, and the angular function is normalized by the values at the interface of the angular function. This means that the stress intensity factor of the interface crack is defined using angular functions for a three-dimensional crack. The stress intensity factor will be investigated along the crack front. Additionally, an expression for the variation in the stress intensity factor against the distance from a singular point, which is the intersection of the crack front with the free surface, will be derived, and its validity will be demonstrated by comparing the two results.

2. Method for analysis

In the present paper, the stresses and displacements in a three-dimensional elastic body will be calculated using a boundary integral equation,

$$u_i(q) = \int_{\Omega} [U_{ij}(q, Q) t_j(Q) - T_{ij}(q, Q) u_j(Q)] ds(Q) \quad (3)$$

where q is an inner point in the domain Ω , Q is a point on the boundary Γ , and U_{ij} and T_{ij} are the fundamental solutions for the displacement and traction, respectively. Here, Rongved's solution,

which is satisfied with the boundary condition of the interface (such as the continuity of stress and displacement), is employed in the analysis (Rongved, 1955). Hence, mesh division on the interface is not required, and accurate stress distributions are then obtained. The stress in the domain Ω is calculated by substituting the displacement gradient into Hooke's law,

$$u_{ij}(q) = \int_{\Omega} [U_{ikj}(q, Q)t_k(Q) - T_{ikj}(q, Q)u_k(Q)] ds(Q) \quad (4)$$

where U_{ikj} and T_{ikj} are the derivatives of the fundamental solutions U_{ik} and T_{ik} at the inner point q .

Next, a method for determining the order of the stress singularity at a singular point is briefly explained (Pageau and Bigger, 1995). There are several singular points in the present joints. Introducing a spherical coordinate system at a singular point, such as a vertex, a sphere of radius r_0 surrounding the singular stress point is considered. Then the displacement fields governed by the singular stress fields in the sphere can be expressed by a power law of the distance from the singular point, where the index of the power law is denoted p . The surface of the sphere is divided into rectangular finite elements, and the displacements in the quadrangular pyramid composed of the vertex and eight nodes on the surface of the sphere are expressed using the power law of the distance and an interpolation function as follows:

$$u_j = \left(\frac{r}{r_0}\right)^p \sum_{i=1}^8 H_i u_{ji} = \rho^p \sum_{i=1}^8 H_i u_{ji} \quad (5)$$

where H_i represents the interpolation function, and u_{ji} is the displacement at node i .

The displacement vectors are used for formulating the finite element equation based on the principle of virtual work. Then, an eigenequation for p is derived as

$$(p^2[\mathbf{A}] + p[\mathbf{B}] + [\mathbf{C}])\{\mathbf{u}\} = \mathbf{0} \quad (6)$$

where $[\mathbf{A}]$, $[\mathbf{B}]$, and $[\mathbf{C}]$ are matrices composed of the material properties and angles relating to the shape of the joint, and $\{\mathbf{u}\}$ is the displacement vector at the node. After determining the eigenvalue p in Eq. (6), the order of the stress singularity λ is obtained from $\lambda = 1 - p$.

3. Model for analysis

In the present analysis, a three-dimensional joint composed of silicon and resin is considered. Joints with and without a crack at the interface are analyzed. Fig. 2 shows the model for the analysis

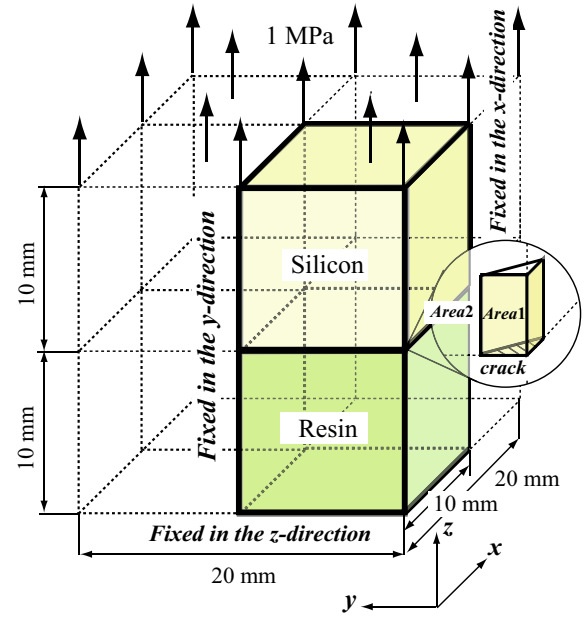


Fig. 2. Analysis model including the size and boundary conditions (the crack area is located at the lower surface in the triangular-column-shaped domain).

and the size of the joint. The upper material is silicon, and the lower material is resin. In this joint model, a very small domain is established for making the crack, and a zone method is employed in the boundary element method (BEM) analysis. Fig. 3 shows the geometry of the interface crack. The height of the small domain is 0.05 mm in the z -direction, and the cross section in the x - y plane is the same size as the interface crack. Here, a triangular-shaped crack is referred to as Type A, a quarter-circular-shaped crack is Type B, and a concave-shaped crack is Type C. The areas of the three types of cracks are equal at $3.618 \times 10^{-8} \text{ mm}^2$. The lengths of the side lines for the three types of cracks and the coordinates of the center of the circle for Type C are $L_a = 2.69 \times 10^{-4} \text{ mm}$, $L_b = 2.15 \times 10^{-4} \text{ mm}$, $L_c = 3.05 \times 10^{-4} \text{ mm}$, $d = 6.82472 \times 10^{-4} \text{ mm}$, and $c = 9.99389648 \times 10^{-4} \text{ mm}$, respectively. A tensile stress of 1 MPa in the z -direction is applied at the upper surface, and the displacement in the z -direction is fixed at the lower surface in the joint model. The upper and lower regions are 10 mm in height and 20 mm in width. A quarter model of the joint is analyzed considering the symmetry of the boundary condition and the geometry. The material properties used in the analysis are shown in Table 1.

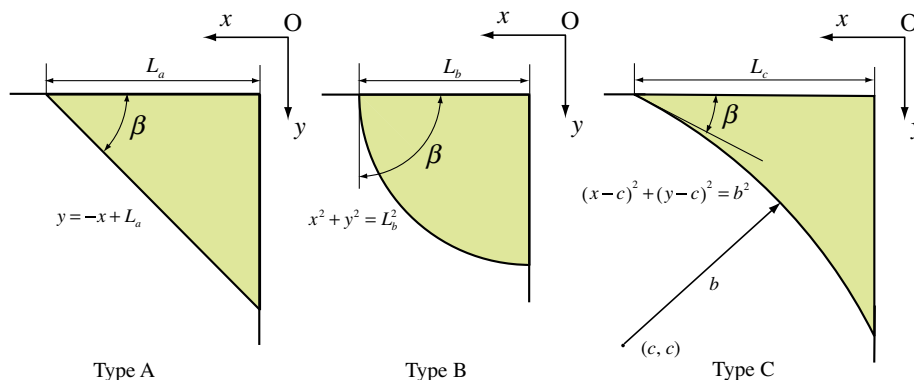


Fig. 3. The shape of the interface crack (Type A: triangular shape, Type B: quarter-circular shape, Type C: concave shape; $L_a = 2.69 \times 10^{-4} \text{ mm}$, $L_b = 2.15 \times 10^{-4} \text{ mm}$, $L_c = 3.05 \times 10^{-4} \text{ mm}$, $b = 6.82472 \times 10^{-4} \text{ mm}$, and $c = 9.99389648 \times 10^{-4} \text{ mm}$).

Table 1
Material properties used in the analysis.

	Silicon	Resin
Young's modulus	166.01	2.74
Poisson's ratio	0.26	0.38

4. Results and discussion

In this section, the stress distributions at the vertexes and around three-dimensional cracks are obtained using the boundary element analysis and precisely discussed. At first, the orders of the stress singularity at several points in the interface and cracks will be obtained. The distributions of the singular stresses will be investigated using the results of eigenanalysis. The stress distribution near the interface crack tip will be expressed using the angular functions determined from the eigenanalysis. The variation of the stress intensity factor defined by the angular functions will be precisely investigated along the three-dimensional crack front.

4.1. Results of eigenanalysis

The orders of the stress singularities at several points on the vertexes and lines including the crack front are needed for investigating the stress intensity factor. The model for the eigenanalysis is shown in Fig. 4. The mesh division for a sphere with a radius r_0 is shown in Fig. 4(a), and the developed meshes on the ϕ and θ planes are shown in Fig. 4(b). The sizes of the elements near the interface and the side surface are reduced. Here, ϕ_{op} means the angle between the side surfaces, and ϕ_{op} is 90° for the vertex and 180° for the singular line. The orders of the stress singularities in the no-crack model are shown in Table 2.

The mesh division for a crack model can be made by setting several different nodes on the interface marked by the red line shown in Fig. 4(b). The crack region is located at $\theta = \pi/2$, $\phi_{op} = 2\pi$, and $0 \leq \phi \leq \phi_c$. The element size used in the analysis is $\theta \times \phi = 9^\circ \times 9^\circ$, and the elements near the interface and the singular stress line are divided into five elements. The orders of the stress singularities are shown in Table 3. Two values are complex numbers, and one is a real number. Furthermore, the order of the stress singularity at the cross point of the crack front line and the side surface is investigated for three types of cracks, and its values are shown in Table 4. There are two values that yield a stress singularity for each type of crack. The values of Type B are larger

Table 2
Eigenvalues for silicon–resin interface.

Stress singularity point, $\phi_{op} = 90^\circ$		Stress singularity line, $\phi_{op} = 180^\circ$	
Re (λ_{vertex})	Im (λ_{vertex})	Re (λ_{line})	Im (λ_{line})
0.395	0.000	0.318	0.000

Table 3
Eigenvalues at a point on the crack front line.

Re(λ_1)	Im(λ_1)	Re(λ_2)	Im(λ_2)	Re(λ_3)	Im(λ_3)
0.50	0.000	0.50	0.0592	0.50	−0.0592

Table 4
Eigenvalues at the intersection S of the crack front and the side surface.

Type A ($\beta = 45^\circ$)		Type B ($\beta = 90^\circ$)		Type C ($\beta = 26.5^\circ$)	
λ_1	λ_2	λ_1	λ_2	λ_1	λ_2
0.317	0.458	0.508	0.673	0.144	0.385

than those of the other types. The values of Type C are the smallest of the three types of cracks.

4.2. Results of BEM analysis

4.2.1. Stress distributions near the vertex – No-crack model

First, the stress distributions near the vertex in the three-dimensional joint with no crack are investigated. The stress components calculated by the BEM in the Cartesian coordinate system are transformed into spherical coordinates with the origin at the vertex. The distributions of the transformed stresses against the distance from the vertex and against the angle from the side surface are shown in Fig. 5(a) and (b), respectively. Here, the suffix of the vertex is added to indicate the stress at the vertex in the model with no crack. In Fig. 5(b), the stresses $\sigma_{\theta\theta}^{vertex}$ and $\sigma_{r\theta}^{vertex}$ are normalized by the stress values at $\phi = 45^\circ$, and $\sigma_{\phi\theta}^{vertex}$ is normalized by the value at $\phi = 30^\circ$. Note that the plotted stresses are parallel to each other and that the slope is -0.395 , which agrees with the result for the vertex of the eigenanalysis shown in Table 2. From a previous study (Koguchi and da Costa, 2010), it is found that the stress distributions near the vertex in a three-dimensional joint can be expressed as

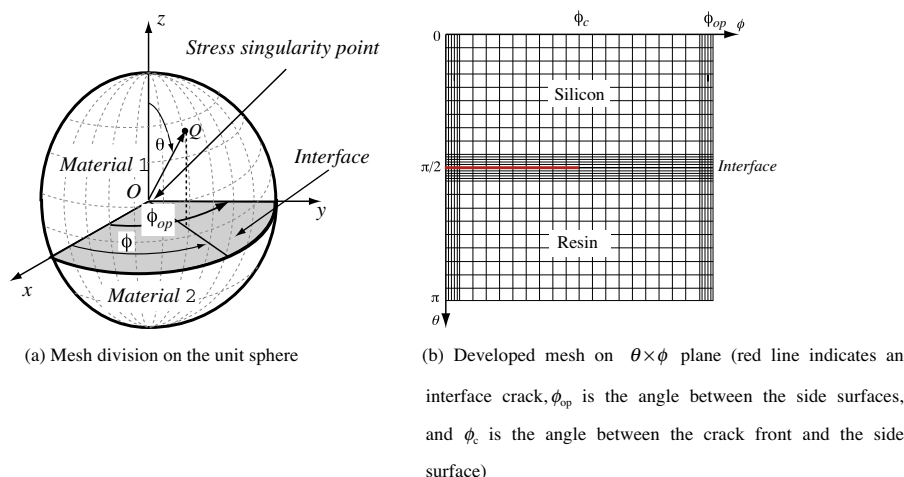
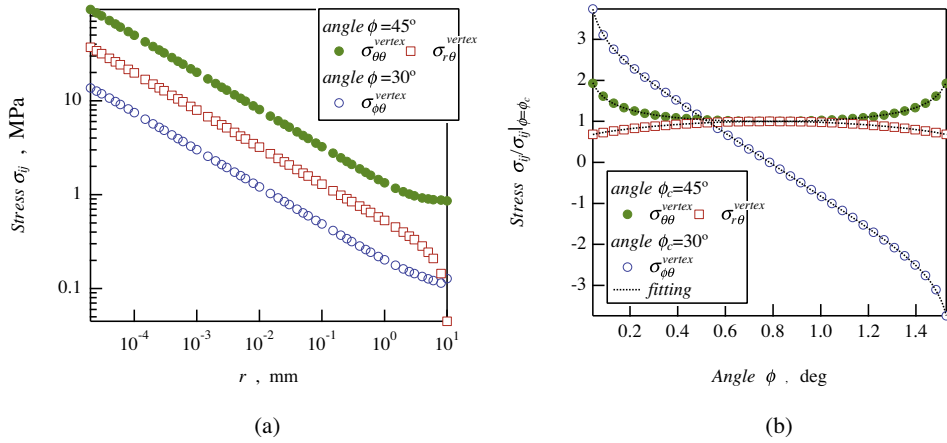


Fig. 4. Finite element mesh for eigenanalysis. (For interpretation of the references to color in this figure legend, the reader is referred to the web version of this article.)



(a) Distributions of $\sigma_{\theta\theta}$, $\sigma_{r\theta}$ and $\sigma_{\phi\theta}$ against the distance, r , from the vertex
 (b) Distribution of $\sigma_{\theta\theta}$, $\sigma_{r\theta}$ and $\sigma_{\phi\theta}$ against the angle ϕ

Fig. 5. Stress distributions near the vertex of the interface.

Table 5
 Values of coefficients in the expressions of stress.

$\sigma_{\theta\theta}^{vertex}$	$K_{100}, \text{MPa} \cdot \text{mm}^{\lambda_{vertex}}$ 1.26	K_{200}, MPa 0.0594	L_{100} 0.64	L_{200} -0.43	–	–
$\sigma_{r\theta}^{vertex}$	$K_{1r\theta}, \text{MPa} \cdot \text{mm}^{\lambda_{vertex}}$ 0.535	$K_{2r\theta}, \text{MPa}$ -0.00154	$L_{1r\theta}$ -0.0298	$L_{2r\theta}$ 0.254	$L_{3r\theta}$ 0.458	–
$\sigma_{\phi\theta}^{vertex}$	$K_{1\phi\theta}, \text{MPa} \cdot \text{mm}^{\lambda_{vertex}}$ 0.194	$K_{2\phi\theta}, \text{MPa}$ 0.0263	$L_{1\phi\theta}$ 1.012	$L_{2\phi\theta}$ 0.826	$L_{3\phi\theta}$ 0.0672	$L_{4\phi\theta}$ 1.919

$$\sigma_{ij}(r, \theta, \phi) = K_{1ij} f_{1ij}(\theta, \phi) r^{-\lambda_{vertex}} + K_{2ij} f_{2ij}(\theta, \phi) \quad (7)$$

where K_{1ij} represents the intensity of the singularity, and $f_{1ij}(\theta, \phi)$ is the angular function for the stress σ_{ij} .

Next, the stress distributions at the interface are precisely investigated. The stress σ_{ij}^{vertex} at the interface is modified as follows:

$$\sigma_{ij}^{vertex}(r, \pi/2, \phi) = K_{1ij} f_{1ij}^{\phi}(\phi) r^{-\lambda_{vertex}} + K_{2ij} f_{2ij}^{\phi}(\phi) \quad (8)$$

The stress distributions shown in Fig. 5(a) are approximated using Eq. (8) by setting the angular functions as $f_{100}^{\phi}(\pi/4) = f_{200}^{\phi}(\pi/4) = 1$ and the intensity of the singularity K_{100} is determined. The coefficients for the other functions are determined in the same manner.

Here, the angular functions at the interface ($\theta = \pi/2$) are expressed as $f_{ij}^{\phi}(\phi)$, which are derived in the previous paper (Koguchi and da Costa, 2010):

$$f_{100}^{\phi}(\phi) = L_{100}(\sin \phi)^{-\lambda_{line}} + L_{200} \quad (9)$$

$$f_{1r\theta}^{\phi}(\phi) = L_{1r\theta} \left\{ (\sin \phi)^{-\lambda_{line}} \cos \phi + (\cos \phi)^{-\lambda_{line}} \sin \phi \right\} + L_{2r\theta} \left\{ (\sin \phi)^{1-\lambda_{line}} + (\cos \phi)^{1-\lambda_{line}} \right\} + L_{3r\theta} \{ \sin \phi + \cos \phi \} \quad (10)$$

$$f_{1\phi\theta}^{\phi}(\phi) = L_{1\phi\theta} \left\{ (\sin \phi)^{-\lambda_{line}} \cos \phi - (\cos \phi)^{-\lambda_{line}} \sin \phi \right\} + L_{2\phi\theta} \left\{ (\sin \phi)^{1-\lambda_{line}} - (\cos \phi)^{1-\lambda_{line}} \right\} + L_{3\phi\theta} \{ \sin \phi - \cos \phi \} \quad (11)$$

where L_{kij} is the coefficient representing the intensity of the singularity for the angular function near the singular stress line.

Furthermore, the coefficients L_{kij} in Eqs. (9)–(11) are determined using the least squares method. The coefficients K_{kij} ($k = 1, 2$) in the singular stress fields are obtained using Eq. (8), and the values of the coefficients are shown in Table 5.

4.2.2. Stress distributions near the vertex – Crack models

Next, the stress distributions in the three-dimensional joints with a crack at the vertex are investigated. Here, a polar coordinate system is set up locally along the crack front line for expressing the stress distributions. Several parameters for the coordinate system are used, as shown in Fig. 6, where O_i ($i = 1, 2, 3, \dots, n$) is the origin of the polar coordinate system, R_i is the distance from the origin O_i in the normal plane of the crack front line, and Θ is the angle from

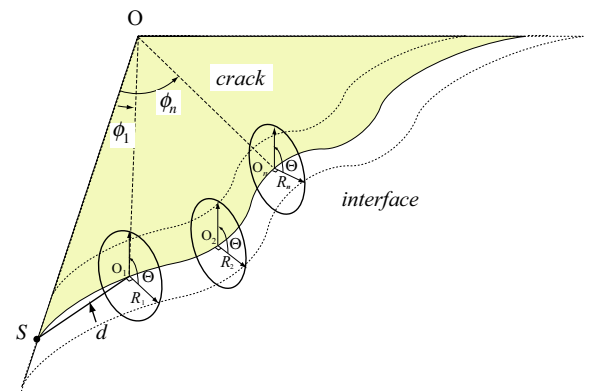


Fig. 6. The local polar coordinate system established along the crack front, and the distance d from the origin to the intersection of the crack front with the side surface.

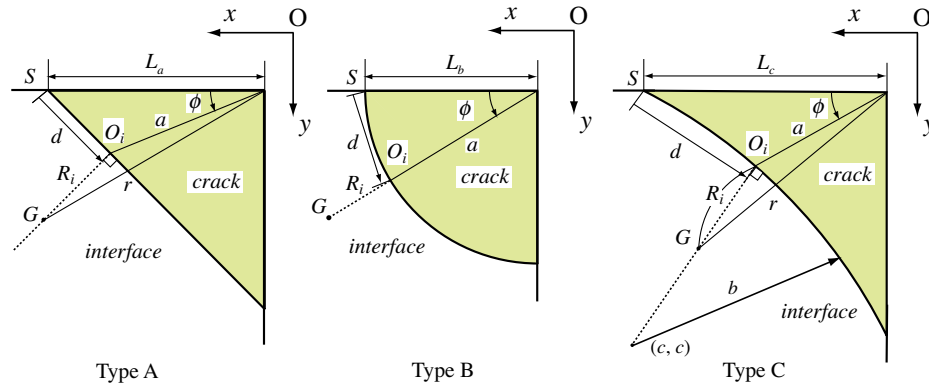


Fig. 7. Polar coordinate system for each crack type.

the interface. The origin O_i is taken at the intersection of the radial vector at an angle ϕ_i from the vertex with the crack front line. Fig. 7 shows the polar coordinate system for each crack shape. The distributions of stress $\sigma_{\theta\theta}$ for the models with a crack and with no crack are demonstrated in Fig. 8(a)–(c) against the distance d from point S . The stress in the model with no crack at a point with a distance R_i far from the crack front line can be calculated by replacing the distance from the vertex r in Eq. (8) by Eq. (12). Here, r for each crack type can be expressed by Eq. (12),

$$r = \begin{cases} \sqrt{R_i^2 + a(\phi)^2 - 2R_i a(\phi) \cos(\frac{3\pi}{4} + \phi)} & (\text{Type A}) \\ a + R_i & (\text{Type B}) \\ \sqrt{R_i^2 + a(\phi)^2 + 2R_i a(\phi) \cos(\phi + \alpha)} & (\text{Type C}) \end{cases} \quad (12)$$

where $\alpha = \tan^{-1} \left(\frac{c - a(\phi) \cos \phi}{c - a(\phi) \sin \phi} \right)$

where $a(\phi)$ represents the crack length at the angle ϕ .

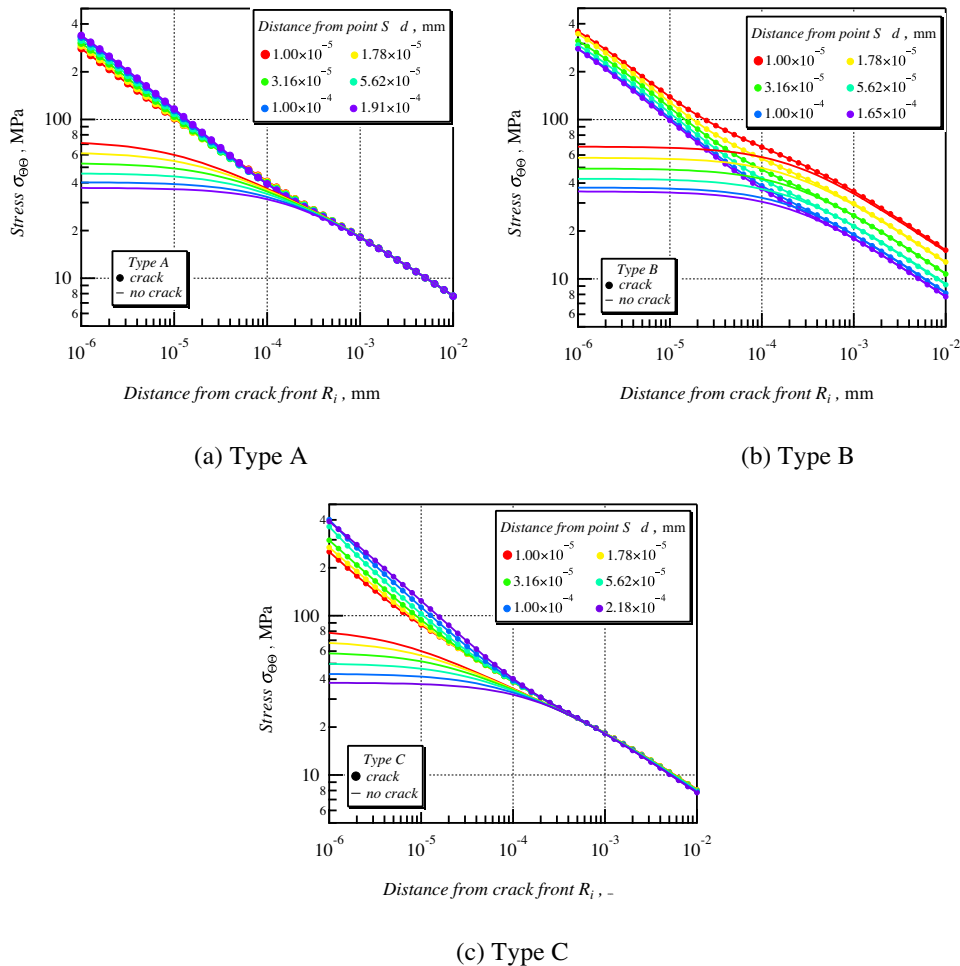


Fig. 8. Distributions of stress $\sigma_{\theta\theta}$ against the distance R_i from the crack front (the symbols indicate the distributions for the model with a crack, and the bars indicate the results for the model with no crack).

The distributions of stress $\sigma_{\Theta\Theta}$ near the crack front in the model with no crack are less than those with a crack, and the slopes of the plots for the no-crack condition are more moderate than those for the crack condition. The slopes of the stress distributions in the models with the crack and with no crack agree well with each other for $R_i > 5 \times 10^{-4}$ mm, and the value of the slope is 0.395, which is the order of the stress singularity at the vertex.

4.3. Stress intensity factors – Mode I

The stress in the crack model is normalized by the stress in the no-crack model, and the distribution of the normalized stress is shown in Fig. 9. It is found that the normalized stress $\sigma_{\Theta\Theta}/\sigma_{\Theta\Theta}^{\text{vertex}}$ is 1 in the range of $R_i > (\text{crack length of the side surface})$ regardless of the distance d from the singular point S . It is supposed that the crack exists in a uniform stress state by normalizing the stress fields near the crack by the stress near the vertex. Furthermore, the distance from the crack front R_i is divided by an arbitrary length ℓ , and then the dimensionless stress field for the results of the eigenanalysis can be expressed as

$$\begin{aligned} \hat{\sigma}_{\Theta\Theta}(\hat{R}, \Theta) &= \sigma_{\Theta\Theta}(\hat{R}, \Theta) / \sigma_{\Theta\Theta}^{\text{vertex}}(\hat{R}, \Theta) \\ &= \hat{K}_{1\Theta\Theta}(\Theta) \hat{R}^{-0.5+i\epsilon} + \bar{\hat{K}}_{1\Theta\Theta}(\Theta) \hat{R}^{-0.5-i\epsilon} + \hat{K}_{2\Theta\Theta}(\Theta) \end{aligned} \quad (13)$$

where $\hat{R} = R/\ell$, $\hat{K}_{1\Theta\Theta}$ is a complex intensity of singularity, $\bar{\hat{K}}_{1\Theta\Theta}$ is a conjugate of $\hat{K}_{1\Theta\Theta}$, and $\hat{K}_{2\Theta\Theta}$ is a real parameter. Here, ℓ is set to 1.0×10^{-6} mm.

$\hat{K}_{1\Theta\Theta}$ is expressed as a product of a real parameter and a complex angular function of Θ as follows:

$$\hat{K}_{1\Theta\Theta}(\Theta) = \hat{K}_1 \tilde{f}_{1\Theta\Theta}(\Theta), \quad \bar{\hat{K}}_{1\Theta\Theta}(\Theta) = \hat{K}_1 \bar{\tilde{f}}_{1\Theta\Theta}(\Theta) \quad (14)$$

where the angular function, $\tilde{f}_{1\Theta\Theta}(\Theta)$, is defined as $\tilde{f}_{1\Theta\Theta}(\Theta) = \tilde{f}_{1\Theta\Theta}^{\text{Re}}(\Theta) + i\tilde{f}_{1\Theta\Theta}^{\text{Im}}(\Theta)$, the conjugate angular function is $\bar{\tilde{f}}_{1\Theta\Theta}(\Theta) = \tilde{f}_{1\Theta\Theta}^{\text{Re}}(\Theta) - i\tilde{f}_{1\Theta\Theta}^{\text{Im}}(\Theta)$, and \hat{K}_1 is a real dimensionless stress intensity factor.

Here, i is an imaginary unit, $\tilde{f}_{1\Theta\Theta}^{\text{Re}}(\Theta)$ and $\tilde{f}_{1\Theta\Theta}^{\text{Im}}(\Theta)$ are real and imaginary parts of the angular function (Hwu and Huang, 2012).

The angular function for the interface crack can be obtained from the eigenvector in the eigenanalysis. Here, the angular function is normalized as follows:

$$\tilde{f}_{1\Theta\Theta}(\Theta) = \frac{f_{1\Theta\Theta}^{\text{Re}} + if_{1\Theta\Theta}^{\text{Im}}}{|f_{1\Theta\Theta}^{\text{Re}} + if_{1\Theta\Theta}^{\text{Im}}|_{\Theta=0}} = \tilde{f}_{1\Theta\Theta}^{\text{Re}} + i\tilde{f}_{1\Theta\Theta}^{\text{Im}} \quad (15)$$

Then, the values of the angular functions at the interface are obtained as $\tilde{f}_{1\Theta\Theta}^{\text{Re}}(0) = 0.527$ and $\tilde{f}_{1\Theta\Theta}^{\text{Im}}(0) = 0.850$. Substituting Eq. (14) into Eq. (13) and arranging the equation yields

$$\hat{\sigma}_{\Theta\Theta}(\hat{R}, 0) = 2\hat{K}_1 \left\{ \tilde{f}_{1\Theta\Theta}^{\text{Re}}(0) \cos(\epsilon \ln \hat{R}) - \tilde{f}_{1\Theta\Theta}^{\text{Im}}(0) \sin(\epsilon \ln \hat{R}) \right\} \hat{R}^{-0.5} + \hat{K}_{2\Theta\Theta}(0) \quad (16)$$

The value of \hat{K}_1 is determined using the least squares method for the stress distributions near the crack front. The relationship

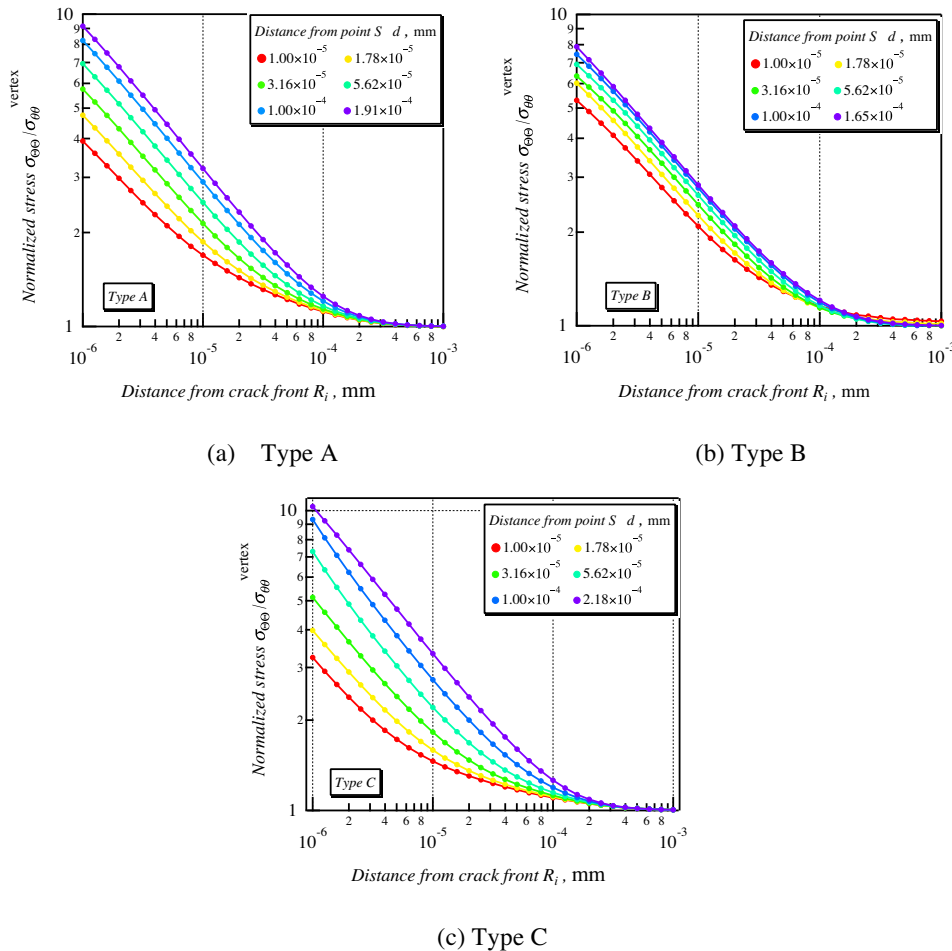


Fig. 9. Distributions of the normalized stress $\sigma_{\Theta\Theta}/\sigma_{\Theta\Theta}^{\text{vertex}}$ against R_i .

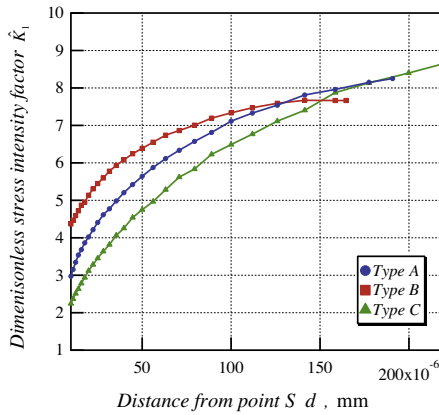


Fig. 10. The distribution of \hat{K}_1 against the distance from point S.

of \hat{K}_1 against the distance d is shown in Fig. 10. The dimensionless, \hat{K}_1 , decreases as the distance d decreases. After that, \hat{K}_1 with a dimension is obtained by multiplying the stress distribution at the vertex, i.e., $K_1 = 2\sqrt{2\pi}\hat{K}_1\sigma_{\theta\theta}^{\text{vertex}}\ell^{0.5}$.

$$\sigma_{\theta\theta}(R,0) = \frac{K_1}{\sqrt{2\pi}} \left\{ \tilde{f}_{1\theta\theta}^{\text{Re}}(0) \cos(\varepsilon \ln \hat{R}) - \tilde{f}_{1\theta\theta}^{\text{Im}}(0) \sin(\varepsilon \ln \hat{R}) \right\} R^{-0.5} + K_{2\theta\theta}(0) \quad (17)$$

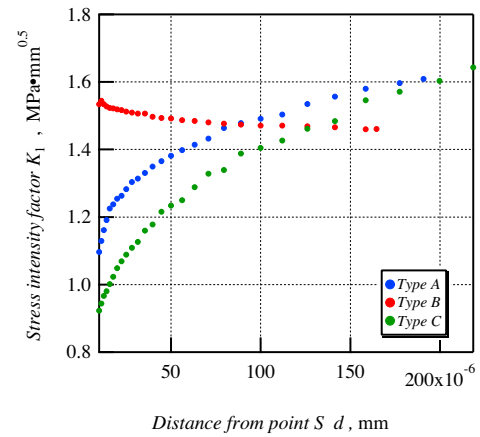
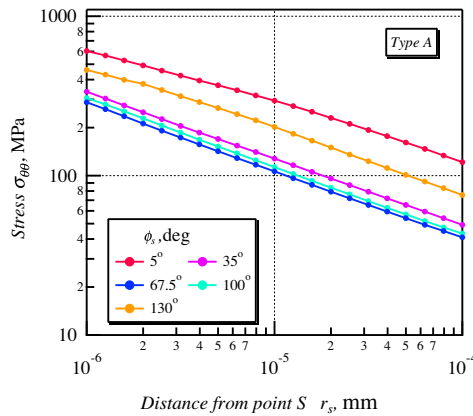
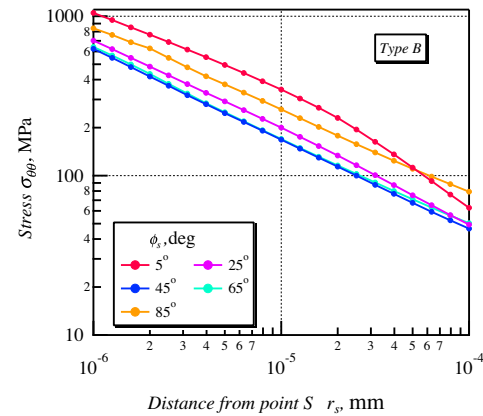


Fig. 11. The distribution of K_1 against the distance from point S.

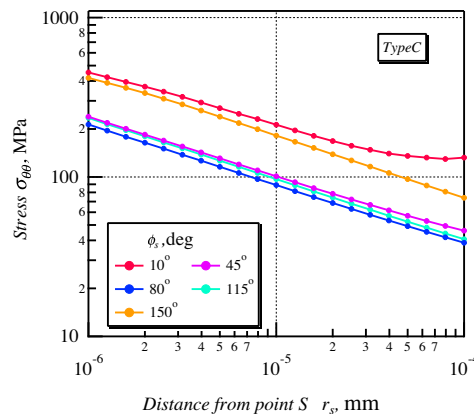
The obtained K_1 is shown against the distance d in Fig. 11. The values of K_1 for Type A and Type C decrease, and K_1 for Type B increases as the angle ϕ decreases. The variation in K_1 against the distance d may be related to the singularity at the cross point of the crack front line and the side free surface because the order of the singularity at point S for Type A and Type C is less than 0.5, and that for Type B is greater than 0.5. Hence, the stress distributions near point S are precisely investigated.



(a) Type A



(b) Type B



(c) Type C

Fig. 12. The distributions of stress $\sigma_{\theta\theta}$ against r_s for each crack type.

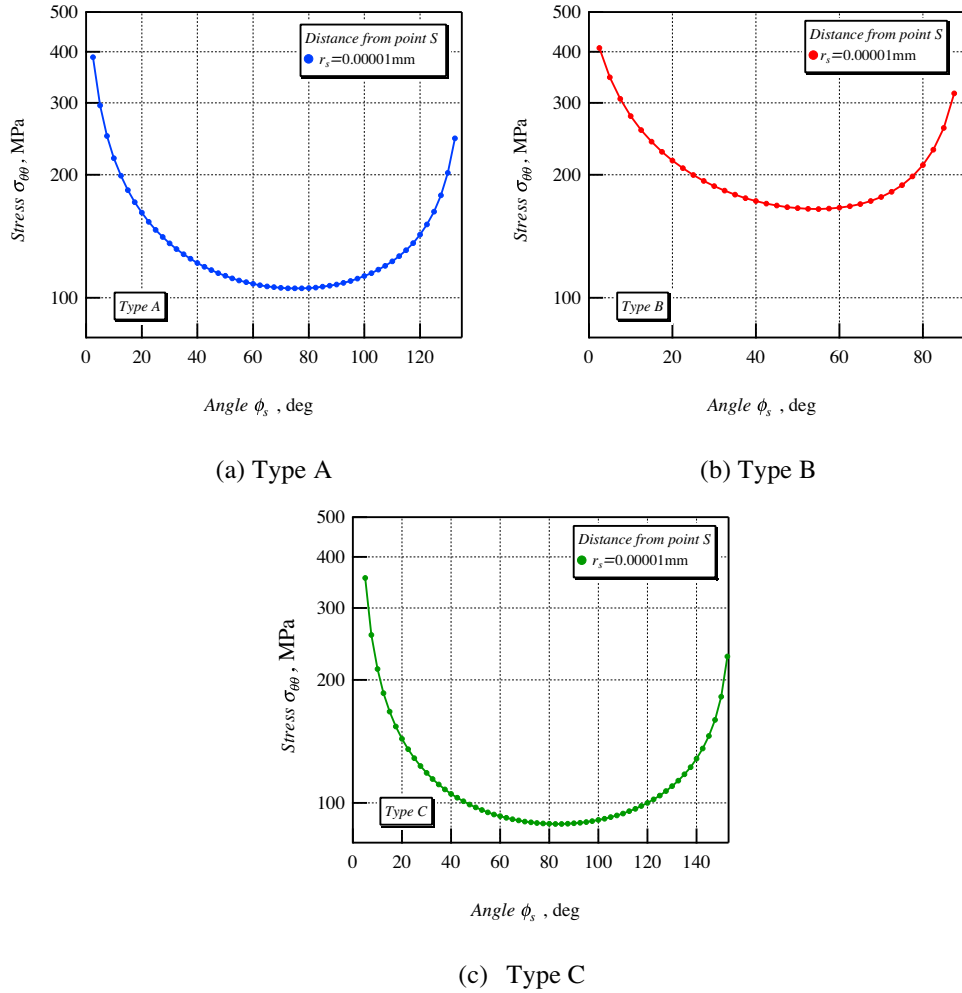


Fig. 13. Distributions of σ_{00} against the angle ϕ_s taken from the crack front.

4.4. Stress analysis at the singular point crossing the crack front line and the side free surface

The stress distributions near the intersection of the crack front line with the side surface are investigated in the spherical coordinate system with the origin at point S. The stress distributions against the distance r_s around the cross point S for each type of crack are shown in Fig. 12. It is found that the stress σ_{00} has singularities that reflect the order of the stress singularity obtained from the eigenanalysis. The distributions against the angle ϕ_s that are taken from the crack front line are shown in Fig. 13. The stress increases as it approaches the free surface and the crack front. This stress behavior relates to the angular function of the stress σ_{00} . Fig. 14 demonstrates the angular functions for each stress singularity value. Here, the angular functions are normalized by each minimum value, which is attained at different angles ϕ_s . Furthermore, the angular functions behave differently near the crack front and the free surface depending on the order of the stress singularity.

The distribution of the stress σ_{00} can be expressed in the same manner as in Eq. (8). Here, σ_{00}^s represents σ_{00} with an origin of the spherical coordinate system at the point S.

$$\sigma_{00}^s\left(\hat{r}_s, \frac{\pi}{2}, \phi_s\right) = K_{100}^s \ell^{-\lambda_1} \tilde{f}_{100}^s(\phi_s) \hat{r}_s^{-\lambda_1} + K_{200}^s \ell^{-\lambda_2} \tilde{f}_{200}^s(\phi_s) \hat{r}_s^{-\lambda_2} + K_{300}^s \tilde{f}_{300}^s(\phi_s) \quad (18)$$

The angular functions $\tilde{f}_{100}^s(\phi_s)$ and $\tilde{f}_{200}^s(\phi_s)$ near the crack front can be expressed as

$$\tilde{f}_{k00}^s(\phi_s) = L_{k00}^{*s} (\sin \phi_s)^{-0.5+ic} + \bar{L}_{k00}^{*s} (\sin \phi_s)^{-0.5-ic} + L_{200}^s \quad (k=1,2) \quad (19)$$

where $L_{k00}^{*s} = L_k^{*s} \{ \tilde{f}_{1\Theta\Theta}^{Re}(0) + i \tilde{f}_{1\Theta\Theta}^{Im}(0) \}$, $\bar{L}_{k00}^{*s} = L_k^{*s} \{ \tilde{f}_{1\Theta\Theta}^{Re}(0) - i \tilde{f}_{1\Theta\Theta}^{Im}(0) \}$. Here, the angular functions for the interface crack are employed. Finally, substituting L_{k00}^{*s} and \bar{L}_{k00}^{*s} into Eq. (19) and expanding the equation yields the following equation:

$$\tilde{f}_{k00}^s(\phi_s) = 2L_k^{*s} \left[\tilde{f}_{1\Theta\Theta}^{Re}(0) \cos\{\varepsilon \ln(\sin \phi_s)\} - \tilde{f}_{1\Theta\Theta}^{Im}(0) \sin\{\varepsilon \ln(\sin \phi_s)\} \right] (\sin \phi_s)^{-0.5} + L_{200}^s \quad (20)$$

Now, a new parameter $L_k^s = 2\sqrt{2\pi} L_k^{*s}$ is introduced.

$$\tilde{f}_{k00}^s(\phi_s) = \frac{L_k^s}{\sqrt{2\pi}} \left[\tilde{f}_{1\Theta\Theta}^{Re}(0) \cos\{\varepsilon \ln(\sin \phi_s)\} - \tilde{f}_{1\Theta\Theta}^{Im}(0) \sin\{\varepsilon \ln(\sin \phi_s)\} \right] (\sin \phi_s)^{-0.5} + L_{200}^s \quad (21)$$

The coefficients L_k^s and L_{200}^s are determined using the least squares method for the distributions of the angular functions near

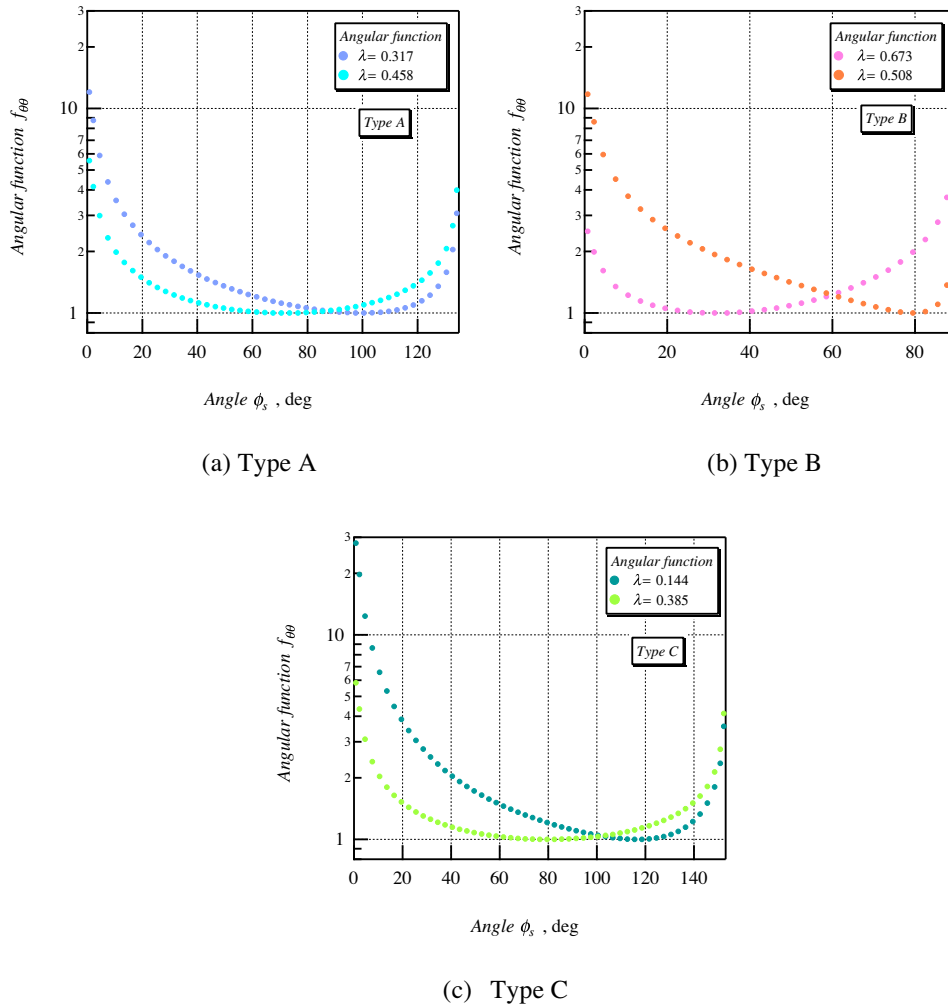


Fig. 14. The angular functions of the interface at point S for each crack type.

Table 6

Values of L_k^s for the angular functions near the crack front.

	Type A		Type B		Type C	
λ_k ($k = 1, 2$)	0.317	0.458	0.508	0.673	0.144	0.385
L_k^s	6.58	2.78	5.97	0.852	16.3	2.93

the crack front shown in Fig. 14. The determined values of L_k^s are shown in Table 6. After that, the intensities of the stress singularity K_{k00}^s corresponding to the orders of the stress singularities, as shown in Table 2, will be determined. However, it is hard to determine two unique unknown values K_{100}^s and K_{200}^s from a distribution for the angle yielding the minimum stress shown in Fig. 15. Here, the solid line represents the stress distribution in the model with no crack, and the solid line with a solid circle shows that in the model with a crack. The stress distribution in the model with no crack is less than that in the model with a crack but has a stress singularity originating from the singular stress line. When the conservative integral developed by Luangarpa and Koguchi (2014) is used, each value of K_{k00}^s ($k = 1, 2$) can be determined separately. A

brief explanation is presented in Appendix A. The obtained coefficients are shown in Table 7. Substituting Eq. (21) into Eq. (18) yields

$$\begin{aligned} \sigma_{\theta\theta}^s(\hat{r}_s, \phi_s) = & \frac{K_{100}^s \ell^{-\lambda_1} L_1^s}{\sqrt{2\pi}} \left[\tilde{f}_{1\theta\theta}^{\text{Re}}(0) \cos\{\varepsilon \ln(\sin \phi_s)\} \right. \\ & \left. - \tilde{f}_{1\theta\theta}^{\text{Im}}(0) \sin\{\varepsilon \ln(\sin \phi_s)\} \right] (\sin \phi_s)^{-0.5} \hat{r}_s^{-\lambda_1} \\ & + \frac{K_{200}^s \ell^{-\lambda_2} L_2^s}{\sqrt{2\pi}} \left[\tilde{f}_{2\theta\theta}^{\text{Re}}(0) \cos\{\varepsilon \ln(\sin \phi_s)\} \right. \\ & \left. - \tilde{f}_{2\theta\theta}^{\text{Im}}(0) \sin\{\varepsilon \ln(\sin \phi_s)\} \right] (\sin \phi_s)^{-0.5} \hat{r}_s^{-\lambda_2} \\ & + K_{100}^s \ell^{-\lambda_1} L_{200}^s \hat{r}_s^{-\lambda_1} + K_{200}^s \ell^{-\lambda_2} L_{300}^s \hat{r}_s^{-\lambda_2} + K_{300}^s \tilde{f}_{300}^s(\phi_s) \end{aligned} \quad (22)$$

4.5. Relationship between K_1 and K_{k00}^s

Here, the variation in the stress intensity factor along the crack front line is investigated using the characteristic of the

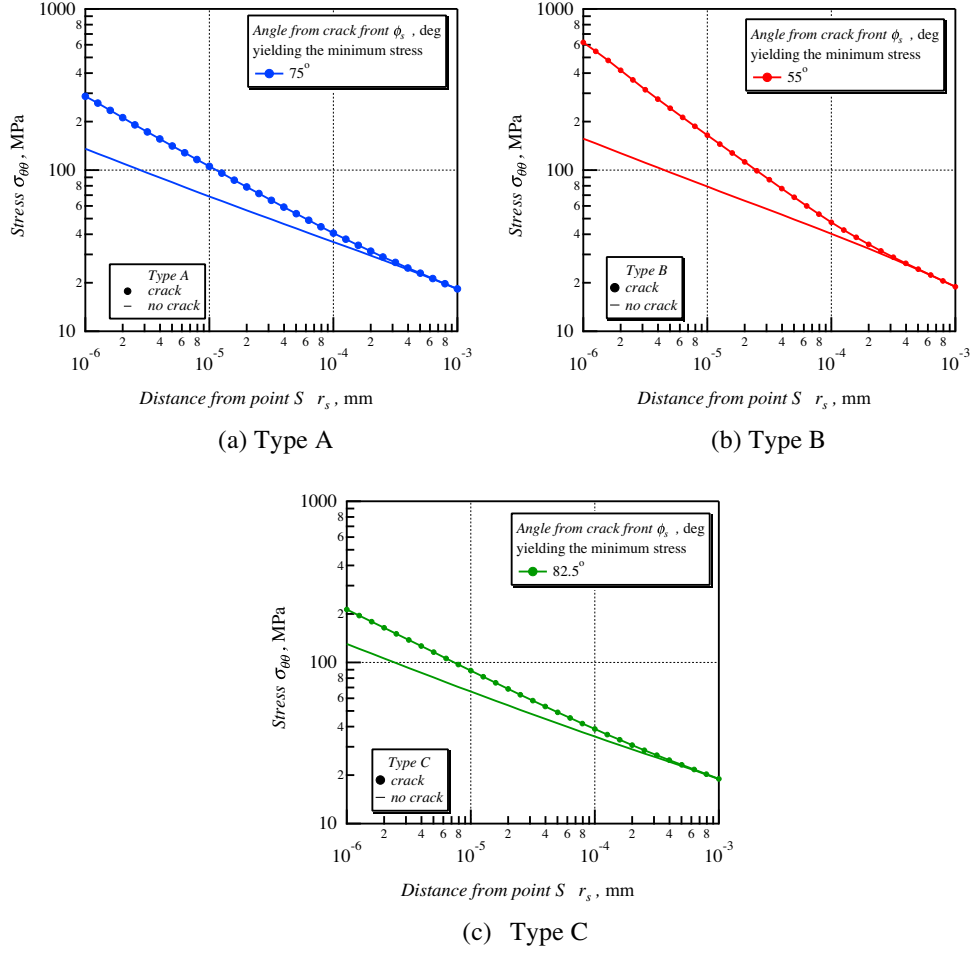


Fig. 15. The stress distribution for the angle ϕ_s yielding the minimum value of the stress (plot with symbols represents the stress in the model with a crack, and the solid line represents the model with no crack).

Table 7
Values of K_{k00}^s at point S.

	Type A		Type B		Type C	
λ_k ($k = 1, 2$)	0.317	0.458	0.508	0.673	0.144	0.385
K_{k00}^s , MPa · mm $^{\lambda_k}$	0.632	0.417	0.205	0.0219	0.771	0.920

singular stress field at point S. When the angle ϕ_s is small, then $\hat{R} = \hat{d} \tan \phi_s \approx \hat{d} \sin \phi_s \approx \hat{d} \phi_s$. Eq. (22) may be modified as follows:

$$\begin{aligned} \sigma_{\theta\theta}^s(\hat{r}_s, \phi_s) \approx & \frac{K_{100}^s \ell^{-\lambda_1} L_1^s}{\sqrt{2\pi}} \left[\tilde{f}_{1\theta\theta}^{Re}(0) \cos\{\varepsilon \ln(\phi_s)\} \right. \\ & \left. - \tilde{f}_{1\theta\theta}^{Im}(0) \sin\{\varepsilon \ln(\phi_s)\} \right] \phi_s^{-0.5} \hat{r}_s^{-\lambda_1} \\ & + \frac{K_{200}^s \ell^{-\lambda_2} L_1^s}{\sqrt{2\pi}} \left[\tilde{f}_{1\theta\theta}^{Re}(0) \cos\{\varepsilon \ln(\phi_s)\} \right. \\ & \left. - \tilde{f}_{1\theta\theta}^{Im}(0) \sin\{\varepsilon \ln(\phi_s)\} \right] \phi_s^{-0.5} \hat{r}_s^{-\lambda_2} \\ & + K_{100}^s \ell^{-\lambda_1} L_{200}^s \hat{r}_s^{-\lambda_1} + K_{200}^s \ell^{-\lambda_2} L_{300}^s \hat{r}_s^{-\lambda_2} + K_{300}^s f_{300}^{\phi}(\phi_s) \quad (23) \end{aligned}$$

and furthermore, $\hat{r}_s \approx \hat{d}$ at $\phi_s \approx 0$, so

$$\begin{aligned} \sigma_{\theta\theta}^s(\hat{d}, \phi_s) \approx & \frac{K_{100}^s \ell^{-\lambda_1} L_1^s}{\sqrt{2\pi}} \left[\tilde{f}_{1\theta\theta}^{Re}(0) \cos\{\varepsilon \ln(\phi_s)\} \right. \\ & \left. - \tilde{f}_{1\theta\theta}^{Im}(0) \sin\{\varepsilon \ln(\phi_s)\} \right] (\hat{d} \phi_s)^{-0.5} \hat{d}^{0.5-\lambda_1} \\ & + \frac{K_{200}^s \ell^{-\lambda_2} L_1^s}{\sqrt{2\pi}} \left[\tilde{f}_{1\theta\theta}^{Re}(0) \cos\{\varepsilon \ln(\phi_s)\} \right. \\ & \left. - \tilde{f}_{1\theta\theta}^{Im}(0) \sin\{\varepsilon \ln(\phi_s)\} \right] (\hat{d} \phi_s)^{-0.5} \hat{d}^{0.5-\lambda_2} \\ & + K_{100}^s \ell^{-\lambda_1} L_{200}^s \hat{r}_s^{-\lambda_1} + K_{200}^s \ell^{-\lambda_2} L_{300}^s \hat{r}_s^{-\lambda_2} + K_{300}^s f_{300}^{\phi}(\phi_s) \quad (24) \end{aligned}$$

The bracket in the first term can be modified as follows:

$$\begin{aligned} & \tilde{f}_{1\theta\theta}^{Re}(0) \cos\{\varepsilon(-\ln(\hat{d}) + \ln(\hat{d} \phi_s))\} \\ & - \tilde{f}_{1\theta\theta}^{Im}(0) \sin\{\varepsilon(-\ln(\hat{d}) + \ln(\hat{d} \phi_s))\} \\ = & \left[\tilde{f}_{1\theta\theta}^{Re}(0) \cos\{\varepsilon \ln(\hat{d})\} + \tilde{f}_{1\theta\theta}^{Im}(0) \sin\{\varepsilon \ln(\hat{d})\} \right] \cos\{\varepsilon \ln(\hat{R})\} \\ & + \left[\tilde{f}_{1\theta\theta}^{Re}(0) \sin\{\varepsilon \ln(\hat{d})\} - \tilde{f}_{1\theta\theta}^{Im}(0) \cos\{\varepsilon \ln(\hat{d})\} \right] \sin\{\varepsilon \ln(\hat{R})\} \quad (25) \end{aligned}$$

Then, the stress distribution at point S can be expressed as

$$\begin{aligned} \sigma_{\theta\theta}^s(\hat{R}, \hat{d}) \approx & \frac{K_{100}^s \ell^{0.5-\lambda_1} L_1^s \hat{d}^{0.5-\lambda_1}}{\sqrt{2\pi}} \left[\left[\tilde{f}_{1\Theta\Theta}^{Re}(0) \cos\{\varepsilon \ln(\hat{d})\} \right. \right. \\ & + \tilde{f}_{1\Theta\Theta}^{Im}(0) \sin\{\varepsilon \ln(\hat{d})\} \left. \right] \cos\{\varepsilon \ln(\hat{R})\} \\ & + \left[\tilde{f}_{1\Theta\Theta}^{Re}(0) \sin\{\varepsilon \ln(\hat{d})\} \right. \\ & - \tilde{f}_{1\Theta\Theta}^{Im}(0) \cos\{\varepsilon \ln(\hat{d})\} \left. \right] \sin\{\varepsilon \ln(\hat{R})\} \left. \right] R^{-0.5} \\ & + \frac{K_{200}^s \ell^{0.5-\lambda_2} L_1^s \hat{d}^{0.5-\lambda_2}}{\sqrt{2\pi}} \left[\left[\tilde{f}_{1\Theta\Theta}^{Re}(0) \cos\{\varepsilon \ln(\hat{d})\} \right. \right. \\ & + \tilde{f}_{1\Theta\Theta}^{Im}(0) \sin\{\varepsilon \ln(\hat{d})\} \left. \right] \cos\{\varepsilon \ln(\hat{R})\} \\ & + \left[\tilde{f}_{1\Theta\Theta}^{Re}(0) \sin\{\varepsilon \ln(\hat{d})\} \right. \\ & - \tilde{f}_{1\Theta\Theta}^{Im}(0) \cos\{\varepsilon \ln(\hat{d})\} \left. \right] \sin\{\varepsilon \ln(\hat{R})\} \left. \right] R^{-0.5} \\ & + K_{100}^s \ell^{-\lambda_2} L_{200}^s \hat{R}_s^{-\lambda_1} + K_{200}^s \ell^{-\lambda_2} L_{300}^s \hat{R}_s^{-\lambda_2} + K_{300}^s f_{300}^{S\phi}(\phi_s) \quad (26) \end{aligned}$$

Comparing the coefficients for the terms $\cos\{\varepsilon \ln(\hat{R})\}$ and $\sin\{\varepsilon \ln(\hat{R})\}$ in Eqs. (26) and (17) yields

$$\begin{aligned} K_{1\Theta\Theta} \tilde{f}_{1\Theta\Theta}^{Re}(0) &= \left(K_{100}^s L_1^s \hat{d}^{0.5-\lambda_1} + K_{200}^s L_1^s \hat{d}^{0.5-\lambda_2} \right) \left[\tilde{f}_{1\Theta\Theta}^{Re}(0) \cos\{\varepsilon \ln(\hat{d})\} \right. \\ & \quad \left. + \tilde{f}_{1\Theta\Theta}^{Im}(0) \sin\{\varepsilon \ln(\hat{d})\} \right] \\ K_{1\Theta\Theta} \tilde{f}_{1\Theta\Theta}^{Im}(0) &= \left(K_{100}^s L_1^s \hat{d}^{0.5-\lambda_1} + K_{200}^s L_1^s \hat{d}^{0.5-\lambda_2} \right) \left[\tilde{f}_{1\Theta\Theta}^{Re}(0) \sin\{\varepsilon \ln(\hat{d})\} \right. \\ & \quad \left. - \tilde{f}_{1\Theta\Theta}^{Im}(0) \cos\{\varepsilon \ln(\hat{d})\} \right] \quad (27) \end{aligned}$$

These equations can be combined as follows:

$$\begin{aligned} K_1^2 \left\{ \left(\tilde{f}_{1\Theta\Theta}^{Re}(0) \right)^2 + \left(\tilde{f}_{1\Theta\Theta}^{Im}(0) \right)^2 \right\} &= \left(K_{100}^s L_1^s \hat{d}^{0.5-\lambda_1} + K_{200}^s L_1^s \hat{d}^{0.5-\lambda_2} \right)^2 \\ & \quad \times \left\{ \left[\tilde{f}_{1\Theta\Theta}^{Re}(0) \cos\{\varepsilon \ln(\hat{d})\} \right. \right. \\ & \quad + \tilde{f}_{1\Theta\Theta}^{Im}(0) \sin\{\varepsilon \ln(\hat{d})\} \left. \right]^2 \\ & \quad + \left[\tilde{f}_{1\Theta\Theta}^{Re}(0) \sin\{\varepsilon \ln(\hat{d})\} \right. \\ & \quad \left. \left. - \tilde{f}_{1\Theta\Theta}^{Im}(0) \cos\{\varepsilon \ln(\hat{d})\} \right]^2 \right\} \quad (28) \end{aligned}$$

where $\left(\tilde{f}_{1\Theta\Theta}^{Re}(0) \right)^2 + \left(\tilde{f}_{1\Theta\Theta}^{Im}(0) \right)^2 = 1$ is used. Finally, the stress intensity factor can be expressed using the intensity of the singularities and the distance d as follows:

$$K_1 = K_{100}^s L_1^s \hat{d}^{0.5-\lambda_1} + K_{200}^s L_1^s \hat{d}^{0.5-\lambda_2} \quad (29)$$

This relationship suggests that the stress intensity factor of mode I varies according to the exponential function of d . Here, K_{k00}^s and L_k^s ($k=1,2$) are determined beforehand from Figs. 14 and 15 using the conservative integral and Eq. (21). Hence, we examine whether the stress intensity factor that is determined from the stress distributions in the polar coordinate system along the crack front line agrees with the relationship on the right side of Eq. (29). The right-hand side of Eq. (29) is referred to as K_{line} . Fig. 16 demonstrates the result of adding the lines of K_{line} to both logarithmic plots of Fig. 11. It is found that the plotted lines agree well with the stress intensity factor K_1 for each crack type. Here, the units of K_1 and K_{k00}^s are $\text{MPa} \cdot \text{mm}^{0.5}$ and $\text{MPa} \cdot \text{mm}^{\lambda_k}$, respectively. It is confirmed that the stress intensity factor K_1 at the interface crack varies near the intersection of the crack front with the free surface following Eq. (29). This relationship will be applied to the other crack shapes. Furthermore, K_{100} for a joint without a crack at $\phi = \pi/4$ is added to Fig. 16. The unit of K_{100} is $\text{MPa} \cdot \text{mm}^{0.395}$, so the values of K_1 and K_{100} cannot be compared generally with each other. However, when we try to compare with both values, in our

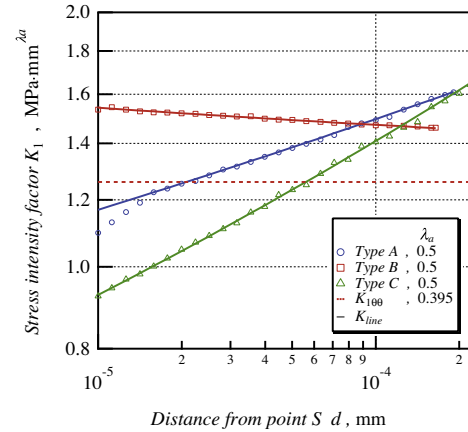


Fig. 16. The relationship between the stress intensity factor K_1 of mode I and the distance from the intersection of the crack front with the free surface. A comparison of K_1 for joints with a crack and K_{100} at $\phi = \pi/4$ for a joint without a crack.

models, the value of d for angle $\phi = \pi/4$ is about 2×10^{-4} mm. The value of the stress intensity factors, K_1 , in Type B is 1.2 times that of K_{100} , and the values in Types A and C are 1.27 times.

It can be said that the values of K_1 are not so much different from the value of the intensity of singularity at the vertex in the present study.

5. Conclusions

In the present study, the singular stress field and the stress intensity factor along the crack front were investigated using the BEM, an eigenanalysis, and the conservative integral. The results are summarized as follows:

1. On the stress near a crack at the vertex in a three-dimensional joint, the singular stress at the vertex is superposed on the stress near the small crack tip.
2. The influence of a small crack on the stress distribution extends to the zone size, which is about 2.5-fold larger than the crack length at the side surface.
3. The variation in the stress intensity factor K_1 of mode I near the side surface along the crack front depends on the order of the stress singularity at the cross point of the crack front and the free surface. When the order of the singularity is less than or greater than 0.5, the stress intensity factor K_1 decreases or increases, respectively, as it approaches the free surface.
4. The stress intensity factor of mode I varies following a function of the distance from the intersection of the crack front and the free surface to a point on the crack front. The function is expressed by the sum of the exponential function with a power index of the difference in the stress singularities at the cross point at the free surface and at the crack tip (0.5).

Acknowledgments

This study has been partly supported by a Grant-in-Aid for Scientific Research (B) 21360051 in Japan. The authors would like to express their sincere gratitude for the support.

Appendix A. A brief explanation of the conservative integral

Here, the conservative integral method for determining the singularity intensity of the singular stress field in a three-dimensional

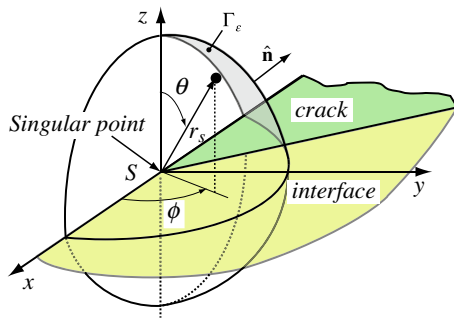


Fig. A1. A semi-sphere with the origin at point S, which is the singular stress point.

joint is briefly explained (refer to Luangarpa and Koguchi (2014) for more details). A conservative integral for a three-dimensional joint is developed using Betti's reciprocal principle as follows:

$$\int_S (T'_i u_i - T_i u'_i) ds = 0 \quad (A1)$$

For any contour S , T_i and T'_i are tractions, and u_i and u'_i are the displacements of the singular and complementary fields. Luangarpa and Koguchi (2014) extended this principle to solve a three-dimensional bi-material model. The conservative integral at the vertex in three-dimensional dissimilar materials is defined as follows:

$$K = \int_{\Gamma_e} (\sigma'_{ij} u_i - \sigma_{ij} u'_i) \hat{n}_j ds \quad (A2)$$

where K is the intensity of the singularity, and Γ_e is an arbitrary surface area enclosing the singular point, as shown in Fig. A1. Eq. (A2) indicates that two sources of the solutions (unprimed and primed solutions) are needed. The unprimed solution is the singular solution with an order of singularity of λ . The BEM is used to calculate the unprimed solutions. On the other hand, the primed solution is the complementary solution with an order of singularity of $\lambda' = 3 - \lambda$. The complementary solution is obtained using FEM eigenanalysis, as shown in Eq. (6).

References

- Akisanya, A.R., Fleck, N.A., 1997. Interfacial cracking from the free-edge of a long bi-material strip. *Int. J. Solids Struct.* 34, 1645–1665.
- Ayhan, A.O., Kaya, A.C., Nied, H.F., 2006. Analysis of three-dimensional interface cracks using enriched finite elements. *Int. J. Fract.* 142 (3–4), 255–276.
- Begley, M.R., Ambrico, J.M., 2001. Delamination of thin films from two-dimensional interface flaws at corners and edges. *Int. J. Fract.* 112 (3), 205–222.
- Bjerkén, C., Persson, C., 2001. A numerical method for calculating stress intensity factors for interface cracks in bimaterials. *Eng. Fract. Mech.* 68 (2), 235–246.
- Chiu, T., Lin, H., 2009. Analysis of stress intensity factors for three-dimensional interface crack problems in electronic packages using the virtual crack closure technique. *Int. J. Fract.* 156, 75–96.
- Dundurs, J., 1969. Discussion: Edge-bonded dissimilar orthogonal elastic wedges under normal and shear loading. *J. Appl. Mech.* 36 (3), 650–652.
- Erdogan, F., 1965. Stress distribution in bonded dissimilar materials with cracks. *J. Appl. Mech.* 32, 403–410.
- Ghahremani, F., Shih, C.F., 1992. Corner singularities of three-dimensional plane interface cracks. *J. Appl. Mech.* 59, 61–68.

- Gosz, M., Dolbow, J., Moran, B., 1998. Domain integral formulation for stress intensity factor computation along curved three-dimensional interface cracks. *Int. J. Solids Struct.* 35 (15), 1763–1783.
- Hirai, H., Chiba, M., Abe, M., Ikeda, T., Miyazaki, N., 2012. Stress intensity factor analysis of an interfacial corner between piezoelectric bimaterials using the H-integral method. *Eng. Fract. Mech.* 82, 60–72.
- Hutchinson, J.W., Suo, Z., 1991. Mixed mode cracking in layered materials. *Adv. Appl. Mech.* 29, 63–191.
- Hwu, C., Huang, H.Y., 2012. Investigation of the stress intensity factors for interface corners. *Eng. Fract. Mech.* 93, 204–224.
- Ioka, S., Matsuda, T., Kubo, S., 2002. A numerical and theoretical study on relationship between stress intensity factor of a small edge crack on interface and free-edge stress singularity of bonded dissimilar materials. *Zairyo* 51, 1373–1379 (in Japanese).
- Johnson, J., Qu, J.M., 2007. An interaction integral method for computing mixed mode stress intensity factors for curved bimaterial interface cracks in non-uniform temperature fields. *Eng. Fract. Mech.* 74, 2282–2291.
- Koguchi, H., da Costa, J.A., 2010. Analysis of the stress singularity field at a vertex in 3D-bonded structures having a slanted side surface. *Int. J. Solids Struct.* 47, 3131–3140.
- Koguchi, H., Kimura, N., 2014. Stress analysis near a small crack within singular stress field in a three-dimensional bonded joint under a tensile load. *Trans. JSME (in Japanese)* 80, 1–14. <http://dx.doi.org/10.1299/transjsme.2014smm0220>.
- Koguchi, H., Hoshi, K., Kurahashi, T., 2012. Analysis for three-dimensional singular stress field at a vertex of bonded interface edge in single lap joint under tensile-shear load. *Trans. Jpn. Soc. Mech. Eng. A* 78, 1558–1574 (in Japanese).
- Kuo, T.-L., Hwu, C., 2010. Multi-order stress intensity factors along three-dimensional interface corners. *J. Appl. Mech.* 77, 031020–031020-12.
- Lee, J.C., Farris, T.N., Keer, L.M., 1987. Stress intensity factors for cracks of arbitrary shape near an interfacial boundary. *Eng. Fract. Mech.* 27 (1), 27–41.
- Leguillon, D., Laurencinb, J., Dupeux, M., 2003. Failure initiation in an epoxy joint between two steel plates. *Eur. J. Mech. A/Solids* 22, 509–524.
- Luangarpa, C., Koguchi, H., 2014. Analysis of a three-dimensional dissimilar material joint with one real singularity using a conservative integral. *Int. J. Solids Struct.* 51, 2908–2919.
- Miyazaki, N., Ikeda, T., Soda, T., Munakata, T., 1993. Stress intensity factor analysis of interface crack using boundary element method – Application of contour-integral method. *Eng. Fract. Mech.* 45 (5), 599–610.
- Nagai, M., Ikeda, T., Miyazaki, N., 2007. Stress intensity factor analysis of a three-dimensional interface crack between dissimilar anisotropic materials. *Eng. Fract. Mech.* 74, 2481–2497.
- Nakamura, T., Kamath, S.M., 1992. Three-dimensional effects in thin film fracture mechanics. *Mech. Mater.* 13 (1), 67–77.
- Ortiz, J.E., Cisilino, A.P., 2005. Boundary element method for J-integral and stress intensity factor computations in three-dimensional interface cracks. *Int. J. Fract.* 133 (3), 197–222.
- Pageau, S.S., Bigger Jr., S.B., 1995. Finite element evaluation of free edge singular stress fields in anisotropic materials. *Int. J. Numer. Methods Eng.* 38, 2225–2239.
- Qu, J., Bassani, J.L., 1993. Interfacial fracture mechanics for anisotropic bimaterials. *J. Appl. Mech.* 60 (2), 422–431.
- Rice, J.R., 1988. Elastic fracture mechanics concepts for interfacial cracks. *J. Appl. Mech.* 55, 98–103.
- Rice, J.R., Sih, G.C., 1965. Plane problems of cracks in dissimilar media. *J. Appl. Mech.* 32, 418–423.
- Rongved, L., 1955. Force interior to one of two joined semi-infinite solids. In: *Proceedings of the First Midwestern Conference Solid Mechanics*, West Lafayette, Indiana, pp. 1–13.
- Sih, G.C., Paris, P.C., Erdogan, F., 1962. Crack-tip, stress-intensity factors for plane extension and plate bending problems. *J. Appl. Mech.* 29 (2), 306–312.
- Song, C., Wolf, J.P., 2002. Semi-analytical representation of stress singularities as occurring in cracks in anisotropic multi-materials with the scaled boundary finite-element method. *Comput. Struct.* 80, 183–197.
- Sukumar, N., Huang, Z.Y., Prevost, J.H., Suo, Z., 2004. Partition of unity enrichment for bimaterial interface cracks. *Int. J. Numer. Methods Eng.* 59, 1075–1102.
- Tvergaard, V., Hutchinson, J.W., 2008. Mode III effects on interface delamination. *J. Mech. Phys. Solids* 56, 215–229.
- Veluri, B., Jensen, H.M., 2013. Steady-state propagation of interface corner crack. *Int. J. Solids Struct.* 50, 1613–1620.
- Williams, M.L., 1959. The stresses around a fault or crack in dissimilar media. *Bull. Seismol. Soc. Am.* 49, 199–204.
- Zhou, W., Lim, K.M., Lee, K.H., Tay, A.A.O., 2005. A new variable-order singular boundary element for calculating stress intensity factors in three-dimensional elasticity problems. *Int. J. Solids Struct.* 42 (1), 159–185.